EurJIC European Journal of Inorganic Chemistry

DOI: 10.1002/ejic.201200322

Metal Complexation of a D-Ribose-Based Ligand Decoded by Experimental and Theoretical Studies

Federico Cisnetti,*[a][‡] Jean-Didier Maréchal,[b] Magali Nicaise,[c] Régis Guillot,[a] Michel Desmadril,[c] François Lambert,[a,d,e,f] and Clotilde Policar*[a,d,e,f]

Keywords: Carbohydrates / Ligand design / Transition metals / Molecular modeling / Density funtional calculations

A combination of experimental and theoretical methods have been used to elucidate the complexation properties of a new sugar-derived hexadentate ligand, namely methyl 2,3,4-tri-*O*-(2-picolyl)-β-D-ribopyranoside (**L**). The coordination bond lengths in the complexes with Mn^{II}, Co^{II}, Ni^{II}, and Zn^{II} show substantial deviations from ideal octahedra with deformation towards trigonal-prismatic geometries, which is indicative of a conformationally constrained ligand. The metal-cation–ligand interactions were studied for **L** and the acyclic analogue **L′** [1,2,3-tri-*O*-(2-picolyl)-1,2,3-propanetriol] by spectroscopic methods and isothermal calorimetric titrations for the series Mn^{II}, Co^{II}, Ni^{II}, Zn^{II}, and Cu^{II}. The results indicate a stabilization of the complexes obtained with **L** compared with **L′**, depending on the nature of the metal. Molecular modeling studies showed that the presence of the sugar moiety strongly favors conformations compatible with metal binding, which suggests an entropic origin of the stabilization of **L** complexes with regards to **L′** complexes. Moreover, the differences in the metal chelation profiles of **L** and **L′** are related to the constraints in the sugar group in the metal-bound structures. This study shows that foreseeing the degree of preorganization of flexible ligands may drive the design of a new generation of chelating compounds.

Introduction

In many ways, a close analogy can be sketched between metal complexation and other host–guest interactions.[1] To describe them both, several molecular variables have to be taken into account. One of the most complex variables is the relation between the conformational flexibility of the ligand and the binding strength of the metal cation. For ligands with a reduced number of low-energy conformations, relatively straightforward estimations of the binding affinity of metal cations as well as a direct correlation between structural and thermodynamic data[2] are accessible. However, for ligands with a high number of degrees of freedom, the correct orientation of the chelating groups becomes one of the main issues in metal-ion recognition processes.[3] According to the original definitions by Cram[4] of ligands as hosts and metal cations as guests, complementarity, the absence of binding-induced strains in the host, and preorganization, in which the host and guest are already organized for binding prior to interaction, are difficult to address in such systems. In these cases, several experimental approaches can provide evidence for the metal binding and selectivity. Computational studies can also facilitate a detailed understanding of the processes that occur at the molecular level. The application of computational methods to inorganic compounds has already led to numerous successes in predicting the impact of the conformation of ligands on metal binding and hence on the properties of complexes.[5] However, novel protocols are needed for large multidentate systems for which ligand folding may have a major impact on the binding process. Indeed, it is expected that the ligand will have a large conformational space, as well as numerous desolvation intermediates corresponding to different accessible metal coordination states. Simulating all these molecular events remains highly challenging. Methods that accurately reflect the electronic properties of transition metals, that is, ab initio or DFT quantum mechanical calculations[6] or force-field methods that account for some electronic character of metals,[7,8] are still limited in reproducing folding processes. Those allowing extensive conformational exploration, such as standard force-field

[a] Institut de Chimie Moléculaire et des Matériaux d'Orsay, UMR CNRS 8182, Université Paris-Sud 11, Bât. 420, 91405 Orsay, France
[b] Unitat de Química Física, Departament de Química, Universitat Autònoma de Barcelona, 08193 Bellaterra, Barcelona, Spain
[c] Institut de Biochimie et de Biophysique Moléculaire et Cellulaire, UMR CNRS 81619, Université Paris-Sud 11, Bât. 430, 91405 Orsay, France
[d] Laboratoire des BioMolécules, Université Paris 6 CNRS-UMR7203, Département Chimie de l'ENS, 24, rue Lhomond, 75231 Paris Cedex 05, France
Fax: +33-1-44323389
E-mail: clotilde.policar@ens.fr
[e] Université Pierre et Marie Curie Paris 6, 4, Place Jussieu, 75005 Paris, France
[f] CNRS, UMR7203 24, rue Lhomond, 75005 Paris, France
[‡] Current address: ICCF-UMR CNRS 6296, Université Blaise Pascal, 63000 Clermont-Ferrand, France
Supporting information for this article is available on the WWW under http://dx.doi.org/10.1002/ejic.201200322.

methods, can reproduce more easily the folding space, but are inaccurate for modeling different metal coordination steps along the binding process.

Carbohydrates are one of the most readily available class of biomolecules in nature and are considered as renewable feedstock for fine chemical synthesis.[9] Even though the conformational properties of chiral carbohydrates are widely used in organic synthesis,[10] their rational use as scaffolds to organize Lewis bases for metal complexation is still rarely exploited.[11] Metal complexes derived from chemically modified carbohydrates[12] most frequently comprise a coordinating core with appended sugar moieties,[13] the latter not being involved in the tuning of the metal binding. Applications of such complexes range from therapeutics[14] to asymmetric catalysis.[15] We have recently shown that sugar moieties can serve as a modular platform for the complexation of transition-metal cations. In this so-called glycoligand strategy the sugar affords a well-defined coordination site for the metal atom. The first examples of this family of ligands were monosaccharides bearing three 2-picolyl ether moieties,[16–20] and the concept was further extended to derivatives of aminodeoxymonosaccharides.[21,22] Considerations of the sugar-ring conformations, as deduced by X-ray structural analysis, were used to rationalize magnetic anisotropy,[17] circular dichroism signatures,[18,21] partial coordination of the ligand to the metal cation,[19] and the formation of supramolecular structures.[22] The synthetic versatility of the glycoscaffold has recently been exploited for regioselective functionalization with fluoro-ionophores and hydroxamates leading to artificial glycosiderophores.[23] The remarkable properties of the glycocomplexes suggest that their conformational and dynamic properties have a large impact on the metal-binding process.

In this article we report a detailed case study of the conformational implications of a glycoligand derived from a new scaffold, namely methyl 2,3,4-tri-*O*-(2-picolyl)-β-D-ribopyranoside (**L**), on the metal selectivity by both experimental and theoretical methods. This ligand bears the coordinating 2-picolyl ether moieties in 1,2,3 relative endocyclic positions in contrast to previously reported ligands containing a 1,2,4-tri-*O*-2-picolyl moiety, that is, with one of the picolyl ether moieties in an exocyclic position.

Polyol–metal complexes have been extensively studied,[24,25] and their properties are closely related to those of glycoligands in which the ether groups are coordinated to the metal cation. It is known that in the polyol series, the α,β,γ axial–equatorial–axial (ax–eq–ax) arrangement of hydroxy groups is one of the highest-affinity metal-complexation sites. In particular, D-ribose has been shown to display a rich coordination chemistry.[26] Methyl β-D-ribopyranoside crystallizes with the $^1C_4$ sugar-ring conformation, which in fact contains an ax–eq–ax site at the 2,3,4-positions.[27] The metal selectivity of this arrangement has also been evidenced by molecular mechanics and depends mainly on the ionic radii of the metal cations.[28] A sugar-derived ligand based on a methyl β-D-ribopyranoside scaffold thus appeared to be a promising candidate to study in detail the influence of the sugar conformation on the metal binding. To evaluate the impact of the sugar moiety, particularly in terms of preorganization and complementarity, the acyclic ligand 1,2,3-tri-*O*-(2-picolyl)glycerol (**L′**) was also studied.[29]

We report herein the synthesis and experimental study of the ligand **L** and its resulting mononuclear complexes with several 3d late-transition metals. The experimental results include X-ray crystallographic, spectroscopic and isothermal titration calorimetric analyses. Computational studies were performed by using force-field and DFT calculations. A protocol combining Monte Carlo sampling and quantum mechanical calculations was applied to shed light on the entropic and enthalpic contributions to the metal–ligand binding. In addition, theoretical calculations provide the most probable structures of the M–**L′** and Cu–**L** systems. Our results clearly show that the impact of embedding the ribopyranoside scaffold in the ligand induces an important contribution of entropic origin to the overall stabilization of M–**L** over M–**L′** systems.

Results and Discussion

Synthesis of Ligands and Complexes

The synthesis of methyl β-D-ribopyranoside via benzoylated intermediates was published by Jeanloz et al. in 1948[30] and may be considered as a classical procedure in carbohydrate chemistry. Steric crowding of the benzoyl groups and the anchimeric assistance of the 2-*O*-benzoyl group ensure complete β-selectivity of the glycosidation reaction. The last step of the synthesis of **L** is a phase-transfer-catalyzed (PTC) picolylation, as for previously reported glycocomplexes (Scheme 1).[18,20] **L** crystallized slowly (over several weeks) on storage at 4 °C yielding crystals suitable for X-ray diffraction experiments.

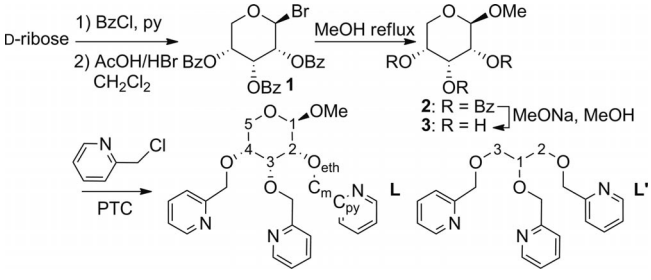

Scheme 1. Synthetic pathway to **L** and **L′** under PTC conditions. Reagents: H_2O/toluene, NaOH, *tert*-amyl-OH, Bu_4NHSO_4. The numbering of the carbohydrate positions in **L** is shown. **L′** was obtained similarly (the synthetic details for **L′** have been published elsewhere).[17]

The M^{II} (M = Mn, Co, Ni, Zn) complexes of **L** were obtained by treating equimolar amounts of the ligand with the M^{II} salts $MY_2{\cdot}6H_2O$ in ethanolic solution (M = Co, Ni, Y = NO_3^-; M = Mn, Zn, Y = ClO_4^-, NO_3^-). When Y = ClO_4^-, precipitation was observed immediately, whereas for Y = NO_3^-, a precipitate was obtained by counteranion metathesis with NH_4PF_6. The salts of the four complex cations

could be redissolved by addition of acetone and crystallized by slow concentration to yield crystals suitable for X-ray analysis. The structures of $[M(\mathbf{L})]Y_2$ ($Y = ClO_4^-$, PF_6^-) have been solved (see below), but attempts to obtain crystalline Cu^{II} complexes were unsuccessful, and no solids could be obtained by treating $\mathbf{L}'$ with M^{II} (M = Mn, Cu, Co, Ni, Zn) salts by similar protocols.

X-ray Structural Studies

Unlike methyl β-D-ribopyranoside, **L** crystallizes in a $^4C_1$ chair conformation with an equatorial OMe group and an eq–ax–eq arrangement at the 2,3,4-positions, inappropriate for coordination (Figure 1). However, reports in the literature reveal that the difference in stability between $^4C_1$ and $^1C_4$ chairs is small. In particular, there are several examples of β-D-ribopyrano derivatives that have different conformations in the solid phase and in solution.[31] Switching between $^4C_1$ and $^1C_4$ chairs would convert the 2,3,4 eq–ax–eq moiety into an ax–eq–ax site, appropriate for coordination (see above).

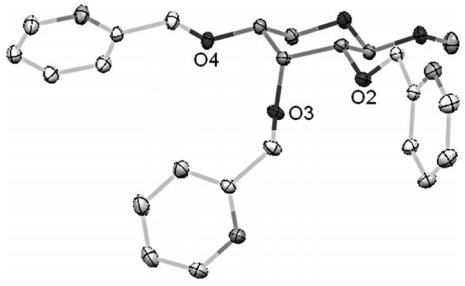

Figure 1. Mercury CCDC[32] plot of the structure of **L**. Ellipsoids are shown at the 50% probability level with the ribopyranose moiety highlighted. H atoms have been omitted for clarity.

In the structures of $[M(\mathbf{L})]Y_2$, the ligand is in the $^1C_4$ ring conformation irrespective of the nature of the cation. Such a conformation results in an ax–eq–ax coordinating arrangement of the three ether moieties. **L** thus defines a neutral *fac*-N_3O_3 coordination sphere with O_{eth},O_{eth} and O_{eth},N chelate cycles. The O_{eth},N chelates are helically folded around the metal cation, thus defining a chirality element that can be described by the Δ/Λ descriptors, as for tris(bidentate) chelates. Different helical configurations were observed depending on the metal, as exemplified in Figure 2 (M = Co, Zn). Moreover, for Mn^{II} and Ni^{II} several different cationic complexes displaying Δ and Λ helical configurations were observed in the crystal lattice (see Figures S1 and S2 in the Supporting Information). In contrast, previously published glycoligands bearing three 2-picolyl ether groups in the 1,2,4 relative positions invariably led to the observation of a single helical configuration in the solid state.[17,18] The lack of coordination stereochemical control by **L** is in line with its quasi-symmetric character: If the OMe group in the 1-position were removed, the ligand would contain a symmetry plane. Structural data for the metal complexes are presented in Table 1. Detailed crystallographic data are collected in the Supporting Information.

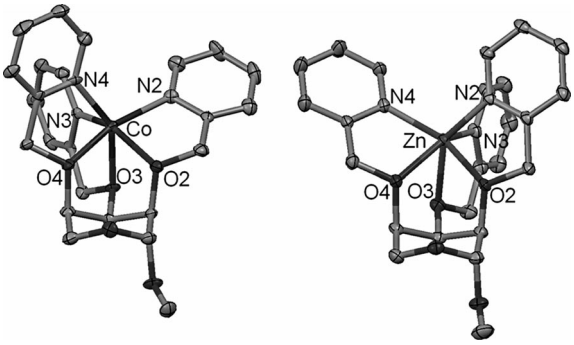

Figure 2. Mercury CCDC[32] plots of the structures of $[Co(\mathbf{L})]^{2+}$ (left) and $[Zn(\mathbf{L})]^{2+}$ (right) in the crystals of $[Co(\mathbf{L})](PF_6)_2$ and $[Zn(\mathbf{L})](ClO_4)_2$, respectively. Ellipsoids are shown at the 50% probability level. H atoms and counterions have been omitted for clarity.

As in one of our previous studies,[18] we adapted the definition of the azimuthal angles[35] for the description of our structures (Scheme 2) to characterize the distortion from octahedral (Θ = 60°) towards trigonal-prismatic geometries (Θ = 0°). In the case of complexes of **L**, there is a pronounced deformation towards the trigonal-prismatic geometry. As shown in Table 1, the distortion is larger for the Mn^{II} (d^5) and Zn^{II} (d^{10}) cations, which display no electronic preference due to their half-filled or filled d orbitals. In terms of the variation of the ligand-field stabilization energy (LFSE), Δ(LFSE) = 0 for Mn^{II} and Zn^{II} between the octahedral and trigonal-prismatic environments, whereas this term may disfavor a trigonal-prismatic geometry for the other metal cations considered here, which vary in the order Δ(LFSE, Co^{II}) = Δ(LFSE, Cu^{II}) < Δ(LFSE, Ni^{II}).[36] Indeed, the Θ_{ave} values (Table 1) follow this trend, which indicates that there is a balance between the LFSE and confor-

Table 1. Structural data for the $[M(\mathbf{L})]Y_2$ complexes.

M	Mn	Co	Ni	Zn
n[a]	2	1	4	1
Helical chirality	Λ/Δ	Δ	2Λ/2Δ	Λ
Θ_{ave}	16.4	30.7	41.4	24.0
Ionic radii[33] [Å]	0.97	0.88	0.82	0.89
Cremer–Pople puckering parameters:[34] QT [Å], θ [°], ϕ [°]	0.525, 173.0, 127[b]	0.529, 175.5, 115	0.539, 175.5, 194[b]	0.539, 176.1, 132
d_{M-O} avg. [Å]	2.253	2.131	2.09	2.196
d_{M-N} avg. [Å]	2.213	2.091	2.03	2.080
$d_{Oeth-Oeth}$[c] [Å]	2.667	2.628	2.646	2.634

[a] Number of nonequivalent cationic units in the lattice. [b] Average value for the nonequivalent cationic units in the crystal lattice. [c] Average distances between picolyl ether oxygen atoms.

mational preferences of the sugar-derived ligands. One may tentatively hypothesize that **L** is accordingly best suited to Mn and Zn and worst suited to Ni^{II}. This loosely correlates with experimental enthalpic trends (see below). However, discussion involving LFSE alone is not sufficient to rationalize the ligand binding.

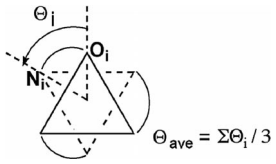

Scheme 2. Definition of the azimuthal angles (adapted from ref.[35]).

As far as the conformation of the pyranoside ring is concerned, the Cremer–Pople puckering parameters[34] can be compared with those of the free ligand **L** (QT = 0.5965 Å, θ = 4.94°). These values are similar to those computed for the crystal structure of methyl β-D-ribopyranoside[27] (QT = 0.5666 Å, θ = 176.23°; a difference of 180° was expected upon ring inversion). Chair-like conformations are observed, resulting in a narrow distribution of average $d_{Oeth–Oeth}$ distances in the range 2.62–2.67 Å between the picolyl oxygen atoms in chelating mode (see Table 1 and below for comparison with calculated structures). Note that the size of the coordinating cavity is determined by these inter-oxygen distances. Indeed, in the case of the $^4C_1$ chair conformation, as in the uncoordinated **L**, the three oxygen atoms are further apart from each other than in the $^1C_4$ chair conformation (see below).

The complexes show distortions from the octahedral and prismatic hexacoordinate geometries with the M–O_{eth} bonds being longer than those of M–N and the O_{eth},O_{eth} and O_{eth},N chelate angles being smaller than 90° (see detailed structural data in Tables S2–S4 in the Supporting Information). The M–N and M–O distances do not simply follow the trend predicted by the hierarchy of the ionic radii. The most notable exception is observed for the zinc complex in which the Zn–O distances are 0.06 Å longer than the Co–O distances despite the fact that the ionic radii of the Co^{II} and Zn^{II} cations differ by only 0.01 Å.[33] The Zn atom is displaced by 0.346 Å from the center of mass of the coordinating atoms in the direction of the N_3 face of the coordination octahedron, leading to a distorted octahedron. This is in line with the fact that a d^{10} cation has no geometric preferences. All these geometric deviations from octahedral coordination suggest an influence of the rigid nature of the ribopyranoside scaffold of **L**. This prompted us to investigate in depth the complexation behavior of **L** and its acyclic analogue **L′**. In the studies that are reported hereafter, we focus on the structural variability of the ligand scaffolds and on the stabilities of the complexes.

NMR Analysis

Ligands and complexes with significant degrees of freedom can exhibit substantial structural differences in the solid state and solution. Therefore, the conformation of the sugar ring in solution was investigated by conventional ^1H NMR techniques both for **L** and its $[Zn(\mathbf{L})]^{2+}$ diamagnetic complex. The ^1H NMR spectra of **L** and $[Zn(\mathbf{L})](ClO_4)_2$ both recorded in $[D_3]$acetonitrile are shown in Figure 3.

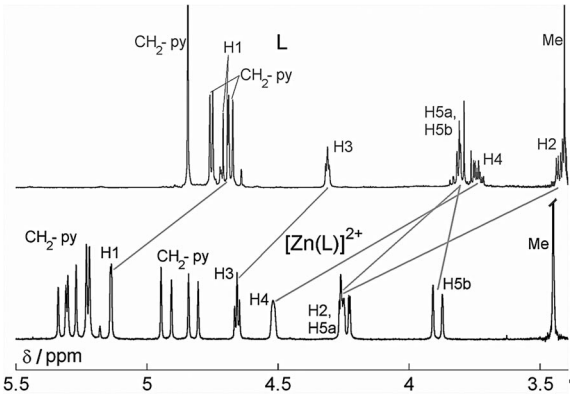

Figure 3. Partial view (signals of the aliphatic protons) of the NMR spectra of **L** and $[Zn(\mathbf{L})](ClO_4)_2$ recorded at 400 MHz in $[D_3]$acetonitrile.

The ^1H NMR spectrum of the complex shows a well-defined set of signals with notable differences in comparison with the ^1H NMR signature of the free ligand. The Haasnoot–Altona equation[37] was used to calculate the $^3J_{H,H}$ coupling constants of the sugar ring by using the dihedral angles obtained from the crystal structures (Table 2). Gratifyingly, good agreement between the experimental and calculated values was obtained. The results show that the most stable sugar-ring conformations of **L** and $[Zn(\mathbf{L})]^{2+}$ in solution are the same as those in the crystal, that is, $^4C_1$ and $^1C_4$, respectively. They also strongly suggest a unique or at least overwhelmingly predominant species for both **L** and $[Zn(\mathbf{L})]^{2+}$. This is further supported by the well-defined ^1H NMR spectrum of the paramagnetic $[Co(\mathbf{L})](PF_6)_2$ (Figure S3). Marked differences in the ^1H chemical shifts between the free ligand and the complex $[Zn(\mathbf{L})]^{2+}$ were observed (Table 3). All the signals of the complex were deshielded relative to those of **L**, but not to the same extent: The protons that are the most deshielded (2-H and 4-H) experience both the proximity of the positive charge of the Zn^{2+} cation[25,38] and a change from an axial to an equatorial position[39] associated with a $^4C_1$ to $^1C_4$ conversion.

Table 2. Selected coupling constantss for **L** and $[Zn(\mathbf{L})]^{2+}$.

	$^3J_{H–H}$ coupling constants [Hz]			
	$[Zn(\mathbf{L})]^{2+}$		**L**	
	Exp.[a]	Calcd.[b]	Exp.[a]	Calcd.[b]
$^3J_{1,2}$	1.5	2.3	6.6	7
$^3J_{2,3}$	3.7	3.3	2.9	2.9
$^3J_{3,4}$	3.7	3.1	2.3	2.6
$^3J_{4,5a}$, $^3J_{4,5b}$	2.0, small[c]	2.7, 1.2	5.1, 7.7	4.8, 9.3

[a] From the ^1H NMR spectra. [b] Calculated with the Haasnoot–Altona[37] equation by using the dihedral angle from the crystal structure. [c] Unresolved.

Table 3. Selected chemical shifts for **L** and $[Zn(\mathbf{L})]^{2+}$.

	δ_H [ppm] $[Zn(\mathbf{L})]^{2+}$	Position	δ_H [ppm] **L**	Position	$\Delta\delta$(cx-lig) [ppm]	d_{H-Zn} [Å][a]
1-H	5.14	eq	4.72	ax	0.42	4.674
2-H	4.26	eq	3.43	ax	0.83	3.631
3-H	4.66	ax	4.31	eq	0.35	3.837
4-H	4.52	eq	3.73	ax	0.79	3.645
5-H	4.25/3.89	eq/ax	3.80	ax/eq	0.45/0.09	4.759/5.034

[a] Distances as determined by X-ray structural analysis

UV/Vis Spectroscopy

UV/Vis titrations were performed to further ascertain the formation of single species of $[M(\mathbf{L})]^{2+}$ upon complexation of the ribose-based ligand. Among the four M^{II} ions forming crystallized complexes with **L**, Co^{II} and Ni^{II} were selected, because they have d–d bands sensitive to the coordination geometry in solution. For cobalt, the addition of **L** results in an increase in the intensity of the UV/Vis bands, and the titration proceeds with a sharp end-point at 1.0 equiv. (Figure S4). More interestingly, in the case of nickel, the spectral changes upon addition of **L** result in clear isosbestic points indicative of a single complexation event (Figure 4). Indeed, the UV/Vis signature of nickel(II) is known to be sensitive to geometric distortions, because they affect the mixing of spectroscopic terms by spin–orbit coupling.[40] As for cobalt, no further spectral changes are observed with excess ligand. These observations further support the presence of a dominant species in solution with a 1:1 metal/ligand stoichiometry for the metal complexes.

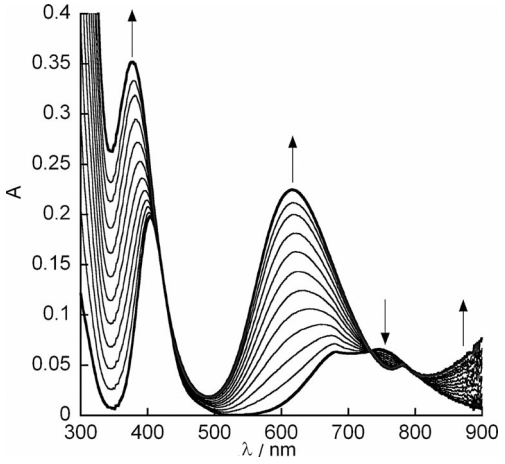

Figure 4. UV/Vis titration of a solution of $Ni(NO_3)_2$ with 0–1 equiv. of **L**. No further changes were detected after the addition of a total of 1.0 equiv. of Ni (10^{-2} mol L^{-1}).

Isothermal Titraction Calorimetry

Isothermal titration calorimetry (ITC), which provides a complete thermodynamic characterization of an interaction in one experiment, is most commonly used in the characterization of interactions between biomolecules. Metal–ligand binding has also been explored (see yearly systematic reviews[41] and references cited therein). When considering metal complexation, ITC is commonly used to study metal-cation–biological macromolecule interactions.[42] The interaction of metal complexes with biological targets has also been investigated by using this technique.[43] In coordination chemistry, studies on the complexation of metal cations by ligands of biological origin,[44] including carbohydrates,[45] or with therapeutic interest[46] have also been reported in the last few years. In a few studies, ITC results have been correlated with structural and other physicochemical data obtained by more common techniques (for recent examples, see ref.[47]).

ITC experiments were undertaken to determine the thermodynamic properties of the complexation of the glycoligand **L** with all the cations for which the structures of the complexes have been resolved by X-ray diffraction and also the Cu^{2+} cation, for which no structure was successfully resolved. To evaluate the impact of the insertion of the hexadentate architecture of the ligand into a pyranose scaffold, identical experiments were carried out on the acyclic analogue of **L**, **L′** (see Scheme 1). Ethanolic solutions of the nitrate salts of the metal cations were titrated against solutions of **L** or **L′** in the same solvent (see the Experimental Section for details). The results of the ITC experiments are summarized in Table 4 and Figure 7. Examples of experimental thermograms are given in Figure S5.

The apparent stabilities of the metal–**L′** complexes follow the conventional Irving–Williams series[48] with Mn < Co < Ni < Cu > Zn. In the case of **L**, a Ni/Cu inversion is observed in the hierarchy of the stabilities of the complexes in comparison with the **L′** series, which indicates that **L** is not very well adapted for Cu^{II} complexation. For a given metal, the complexes of **L** are always more stable than those of its acyclic analogue **L′**. However, the magnitude of the stabilization is dependent on the nature of the metal cation. The effects are less marked than those observed in the series of metal complexes deriving from very rigid ligands (as an example, see a recent study with bicyclic bispidine ligands[49]); however, the results highlight the conformational properties of **L** in fine-tuning metal complexation. The stabilization arising from the pyranose-centered nature of **L** is highest for the two ions that do not display electronic preferences for a given geometry, namely Mn^{II} and Zn^{II}, which can be correlated with the distortions towards trigonal-prismatic geometries observed in the solid-phase structures. Examination of the enthalpic and entropic contributions to the Gibbs energy of formation of the complexes indicates an intricate behavior with subtle effects due to the presence of the sugar moiety. The enthalpic term can be

Table 4. Thermodynamic parameters obtained from isothermal calorimetric titrations.[a]

M	L′	L	Comparison (Δ: L – L′)
Mn	n = 1.34; $K_d = 4.4\times10^{-4}$ ΔH_{exp} = –7.7; $-T\Delta S_{exp}$ = –11.2	n = 1.20; $K_d = 8.1\times10^{-6}$ ΔH_{exp} = –9.2; $-T\Delta S_{exp}$ = –19.2	X = 54.3; $\Delta\Delta H_{exp}$ = –1.5 $-T\Delta\Delta S_{exp}$ = –8.0
Co	n = 0.90 $K_d = 1.9\times10^{-5}$ ΔH_{exp} = –11.6; $-T\Delta S_{exp}$ = –14.9	n = 0.91; $K_d = 2.3\times10^{-6}$ ΔH_{exp} = –14.4; $-T\Delta S_{exp}$ = –17.3	X = 8.3; $\Delta\Delta H_{exp}$ = –2.8 $-T\Delta\Delta S_{exp}$ = –2.4
Ni	n = 1.01; $K_d = 8.9\times10^{-7}$ ΔH_{exp} = –23.2; $-T\Delta S_{exp}$ = –12.1	n = 0.80; $K_d = 2.1\times10^{-7}$ ΔH_{exp} = –12.7; $-T\Delta S_{exp}$ = –26.2	X = 4.2; $\Delta\Delta H_{exp}$ = +10.5 $-T\Delta\Delta S_{exp}$ = –14.1
Cu	n = 0.87; $K_d = 3.6\times10^{-7}$ ΔH_{exp} = –28.1; $-T\Delta S_{exp}$ = –8.1	n = 1.03; $K_d = 2.8\times10^{-7}$ ΔH_{exp} = –23.2; $-T\Delta S_{exp}$ = –13.5	X = 1.3; $\Delta\Delta H_{exp}$ = +4.9 $-T\Delta\Delta S_{exp}$ = –5.4
Zn	n = 0.70; $K_d = 1.1\times10^{-5}$ ΔH_{exp} = –17.3; $-T\Delta S_{exp}$ = –10.7	n = 0.76; $K_d = 3.6\times10^{-7}$ ΔH_{exp} = –13.1; $-T\Delta S_{exp}$ = –23.8	X = 30.6; $\Delta\Delta H_{exp}$ = +4.2 $-T\Delta\Delta S_{exp}$ = –13.1

[a] Addition of a solution of **L** or **L′** in absolute ethanol to a solution of $M(NO_3)_2$ in absolute ethanol at 20 °C. n = experimental stoichiometry, $X = K_d(\mathbf{L}')/K_d(\mathbf{L})$. Units for ΔH_{exp} and $-T\Delta S_{exp}$ are kJ mol^{-1}. An experimental error of ±10% is admitted (by repetition of the same experiment) for K_d and ΔH_{exp}.

either more or less favorable for **L** compared with **L′**. In contrast, the entropic term is always more favorable for the complexation of **L**. These findings can be understood by considering the structures of the ligands, namely the rotation around the bonds common to the chelate cycles and the pyranoside ring, which are blocked in the case of **L**. As degrees of freedom are lost upon coordination, any constraint pre-freezing these degrees of freedom in the free ligand itself is entropically favorable.[1] Enthalpically, the rigidity of the ribose scaffold of **L** may be detrimental in some cases in which the metal geometrical preferences are not matched to those of the ligand or if distances to the metal cation are constrained to a high value. However, the detailed variations in the entropic and enthalpic terms upon complexation is nontrivial. Molecular modeling calculations were performed to shed light on the molecular basis for the metal binding of **L** and **L′**.

Molecular Modeling

An accurate simulation of the binding of metal ions to ligands displaying numerous conformations in solution is still a challenging problem for molecular modeling.[8,50] Exact representations of the full extent of the solvation/desolvation of the separated reactants and the important number of intermediates that could appear in the overall course of the binding[51] are important physicochemical variables for which computational chemistry methods are limited. Combining several molecular modeling techniques can be important for providing a better atomic representation of the metal-binding process if structural variables of interest are appropriately chosen and reasonable assumptions are made.[52] Here, to investigate the molecular basis for the distinct behaviors of **L** and **L′** in metal binding, two different molecular variables were studied independently. The first one is the folding of the ligands and their propensity to adopt conformations adequate for the fixation of the metal atoms in a hexadentate environment. The second is the variation in the binding energy of the different metal cations between $[M(\mathbf{L}')]^{2+}$ and $[M(\mathbf{L})]^{2+}$ complexes. In our modeling study, the first aspect was addressed by Monte Carlo calculations on the unbound ligand and the second by performing full atom functional density theory (DFT) calculations on each of the $[M(\mathbf{L}')]^{2+}$ and $[M(\mathbf{L})]^{2+}$ complexes.

Exploring the Chemical Spaces of the L and L′ Ligands – Evaluation of Preorganization Profiles

Large conformational samplings on each unbound **L** and **L′** ligand were performed by using the torsional Monte Carlo algorithm implemented in the Macromodel package.[53] Calculations were performed with the OPLS force field,[54] including optimized parameters of the sugar as implemented in the Schrodinger distribution. For each ligand, 10000 structures were generated by Monte Carlo (MC) calculation. To determine the number of conformations favorable to metal binding, the molecular ensembles were analyzed on the basis of the average distance between the oxygen atoms of the three picolyl ether groups (O_{eth}). Based on this molecular descriptor, one can see that both **L** and **L′** ensembles are divided into two major subsets (Figure 5).

The first of these subsets contains structures with average O_{eth}–O_{eth} distances between approximately 2.80 and 3.00 Å, and the second contains structures with average distances between 3.30 and 3.75 Å. Detailed analysis shows that the structures of the first subset display their three ethereal picolyl oxygen atoms in a close relative position (ax–eq–ax), as observed in the metal complexes.

However, for the second subset, one of the O_{eth}–O_{eth} distances is always much longer than the others, which is similar to the X-ray structure of the unbound **L** ligand (the average O_{eth}–O_{eth} distance observed for the experimental structure of **L** is about 3.3 Å). It is clear that in the second subset of conformations **L** cannot behave as a hexadentate ligand towards a single metal cation. For this reason, the structures of the first subset can be considered as "bound-like" conformations, whereas those of the second are considered as "free-like" conformations. Strikingly, for the **L** system, all "bound-like" structures display $^1C_4$ ring conformations with an ax–eq–ax site, whereas all "free-like" struc-

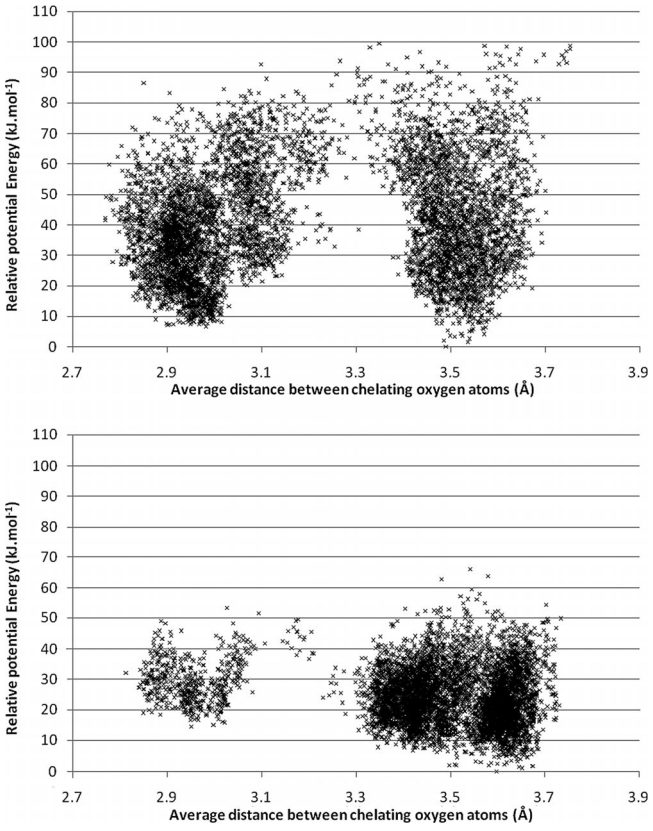

Figure 5. Energy (in kJ mol^{-1}) vs. average of picolyl oxygen distances (in Å) obtained from Monte Carlo simulations for the hexadentate ligands **L** (top panel) and **L′** (bottom panel).

tures display $^4C_1$ conformations with an eq–ax–aq site. This is particularly true for low-energy structures of each subset, whereas intermediate sugar conformations are observed for structures that lie in between the two subsets. The relative populations of "free-like" and "bound-like" subsets are highly dependent on the molecular architecture of the ligand. For **L′**, about 9% of all the structures display "bound-like" conformations, whereas 90% of them display "free-like" ones. In contrast, for **L**, 72% of the structures are "bound-like", and 27% are "free-like". Note also that for the "bound-like" subset, the distances O_{eth}–O_{eth} are in the range 2.9–3.1 Å, whereas in the X-ray structures of the complexes they are slightly shorter (in the range 2.6–2.7 Å). These "bound-like" conformations may thus be considered as being on the path to coordination.

Taking into account the energetic considerations, the difference in energy between the most stable structures of the "free-like" and "bound-like" conformations of **L′** is about 15 kJ mol^{-1} (Figure 5), whereas this difference in **L** is about 8 kJ mol^{-1}. The latter is in agreement with experimental evidence showing that the $^4C_1$ conformation is more stable in solution (see the NMR Analysis section above). Assimilating the potential energy with enthalpic tendencies also highlights the fact that the insertion of the sugar group into the ligand scaffold contributes to a stabilization of "bound-like" conformations. Nonetheless, the most interesting discussion that arises from the Monte Carlo sampling comes in terms of entropic tendencies. To evaluate this magnitude (see the Experimental Section), the variation in entropy for the preorganization of the ligand was calculated by using Equation (1).

$$\Delta S_{preorg.} = S_{bound\text{-}like} - S_{free\text{-}like} \quad (1)$$

For **L′**, the variation in entropy associated with the organization of the ligand in a "bound-like" structure is about –1.47 kJ mol^{-1} K^{-1}, whereas for **L** it is about +0.82 kJ mol^{-1} K^{-1}. The corresponding value of $\Delta\Delta S_{preorg}$ between **L** and **L′** is therefore about 2.3 kJ mol^{-1} K^{-1} in favor of **L**. This result means that the presence of the ribose moiety has a large stabilizing impact on the folding of the hexadentate glycoligand from an entropic point of view. The predicted entropic magnitudes agree with the general tendency observed experimentally as the experimental values of $\Delta\Delta S_{exp}$ range from 8 to 47 J mol^{-1} K^{-1} in favor of **L**. It was impossible to reproduce the exact entropic differences between both ligands. Such discrepancies may arise from limitations of the model in reproducing explicitly the solvent effect, or not accounting for the full extent of the conformational space. However, these calculations demonstrate that the insertion of a sugar moiety in the ligand scaffold induces a large entropic contribution by a conformational restriction within a region favorable for complexation, that is, the sugar scaffold improves ligand preorganization. From this part of the study though we are not able to discuss the molecular basis for the variation of the thermodynamic quantities depending on the nature of the metal.

Density Functional Calculations – Determination of Metal Selectivities of L Versus L′

Quantum mechanical calculations were performed with the B3LYP density functional[55,56] to calculate the binding energies with Equation (2) and the differences in binding magnitudes of each metal to **L** and **L′** ligands with Equation (3).

$$\Delta X_{theo} = X_{complex} - (X_{unbound\ ligand} + X_{isolated\ metal}) \text{ with } X = S \text{ or } H \quad (2)$$

$$\Delta\Delta X_{theo} = \Delta X([M(\mathbf{L})]) - \Delta X([M(\mathbf{L}')]) \quad (3)$$

B3LYP geometry optimizations carried out on $[M(\mathbf{L})]^{2+}$ (with M = Mn, Co, Ni, Cu, and Zn) led to structures in very good agreement with their experimental counterparts when available (all except Cu). In all the optimized structures, the sugar moiety remains in the $^1C_4$ conformation and the metal ion is hexacoordinated to the oxygen and nitrogen atoms of the picolyl ether groups (Figure 6; detailed analyses are reported in the Supporting Information). As no crystal structures are available for $[M(\mathbf{L}')]^{2+}$ systems, B3LYP optimizations were carried out on the structures generated by adding the metal ion to those conformations of the **L′** ligand obtained by the Monte Carlo search and selecting the most suitable structure for metal binding. All

the optimized geometries of the $[M(\mathbf{L}')]^{2+}$ complexes are isostructural with the metal ions in a hexacoordinate environment with trigonal-prismatic geometry (Figure 6). Only subtle structural variations appear between the $[M(\mathbf{L}')]^{2+}$ complexes in the series.

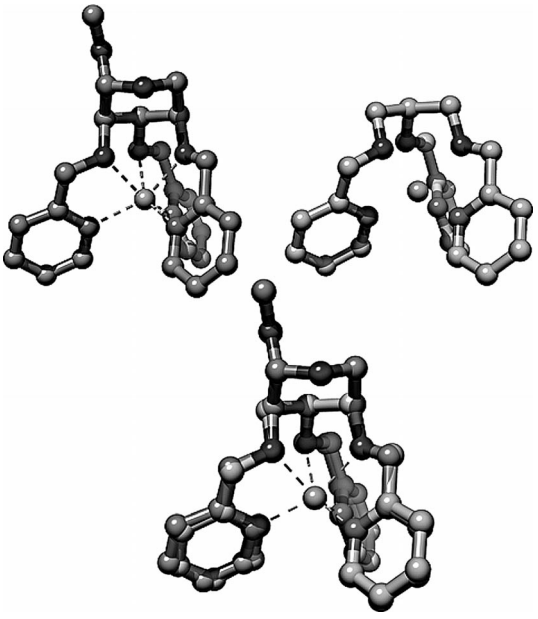

Figure 6. Ball-and-stick representations of representative structures of optimized $[M(\mathbf{L})]^{2+}$ (top left) and $[M(\mathbf{L}')]^{2+}$ (top right) and the best structural overlap between both structures. Examples given for M = Zn.

Comparison between $[M(\mathbf{L})]^{2+}$ and $[M(\mathbf{L}')]^{2+}$ complexes shows very high structural matching (see Figure 6 and the Supporting Information). Indeed, for a given metal, the variations in the M–O and M–N bond lengths between the $[M(\mathbf{L})]^{2+}$ and $[M(\mathbf{L}')]^{2+}$ complexes are less than 0.02 and 0.03 Å, and the average rmsd is about 0.2 Å for all atoms except those from the sugar moiety. These results reveal that the $[M(\mathbf{L}')]^{2+}$ and $[M(\mathbf{L})]^{2+}$ systems provide extremely similar chelating environments to the metal atoms.

To evaluate thermodynamic quantities, geometry optimizations on a "bound-like" conformation of the ligands were also performed. These species were generated by removing the metal ion from the optimized structures of the complexes. Interestingly, the resulting geometries of the optimized **L** and **L**′ ligands are very similar to those of the $[M(\mathbf{L})]^{2+}$ and $[M(\mathbf{L}')]^{2+}$ complexes. In particular, in the structure of **L**, the ribose group remains in the $^1C_4$ conformation and does not converge to the $^4C_1$ structure as observed in the crystalline form of the free ligand. This shows that indeed a preorganized form of this ligand compatible with metal binding represents a stable local minimum and corresponds to a $^1C_4$ conformation. Analysis of the structural features of both **L** and **L**′ ligands and their comparison with their respective complexes reveal that the angle C_{py}–C_M–O_{eth} and O–C_x–C_y–O are particularly sensitive to the nature of the ligand and that the binding of the metal ion should constitute a stronger constraint on **L** than **L**′. This is expected to contribute significantly to the energetic differences observed between the metal binding to **L** and **L**′ (see the Supporting Information).

To extract thermodynamic data for the metal binding to **L** and **L**′, frequency calculations were performed on each of the isolated reactants and products. Theoretical variations in enthalpies of binding between **L** and **L**′ ligands [$\Delta\Delta H_{theo}$ obtained from Equations (2) and (3)] vary between 51.8 and 55.8 kJ mol^{-1}, respectively (Table S8). The general trend in enthalpic preferences for **L**′ versus **L** is in agreement with experiment. Theoretical values of $\Delta\Delta H_{theo}$ (Table 4) are clearly not able to reproduce the exact experimental magnitude but still provide very interesting information. First, they indicate that the constraints in the "bound-like" conformation of the ribose moiety in **L** can result in an enthalpic penalty with respect to the binding of the unconstrained **L**′. The extent of this complementarity effect depends on the bound metal ion. Moreover, the overall enthalpic trend obtained from these calculations reproduces the experimental order for $\Delta\Delta H$, except for the inversion Co/Mn (Figure 7 and Table S8). Analysis of the structural features of both complexes and ligands suggests that these differences in the $\Delta\Delta H$ series are loosely correlated with M–ligand distances, with long distances (Mn, Co, Zn) leading to weaker constraints on the ribose moiety. Because of the small values of $\Delta\Delta H_{exp}$, limitations in both experiment and calculation may explain the differences in absolute values.

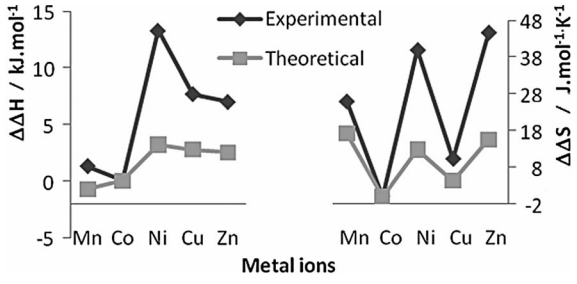

Figure 7. Representation of experimental (ITC) and calculated (DFT) differences in the variation of enthalpy (left) and entropy (right) upon complexation of **L** and **L**′. $\Delta\Delta X = X_{M-L} - X_{M-L'}$ with $X = H$ or S. For ease of interpretation, values are given relative to the cobalt systems.

Computational entropies of binding were calculated by using Equation (1). All the calculated ΔS_{theo} values are negative, irrespective of the ligand or the metal ion, and hence are consistent with the decrease in the number of degrees of freedom upon complexation (Table S7). Clearly, under the experimental conditions, desolvation of both the metal and ligand species is important, which explains the positive values of ΔS_{exp} (from 8 to 48 J mol^{-1} K^{-1}). However, considerable attention has been paid yet again to the values of $\Delta\Delta S$. The trend in differences in entropy of the binding of metal atoms to **L** compared with **L**′ determined theoretically is overall in agreement with experimental data (Figure 7, Table 4, and the Supporting Information). In particular, cobalt and copper represent a first subset with the lowest $\Delta\Delta S_{theo}$ values of –6.7 and –2.4 J mol^{-1} K^{-1},

respectively, whereas manganese, nickel, and zinc represent a second subset with more favorable entropies of binding to **L** of about 8 $J mol^{-1} K^{-1}$ on average. Looking at the first coordination sphere of the metal ions in the different complexes provides an interesting molecular explanation for this phenomenon. Although all M–O distances increase from **L** to **L′**, the M–N distances fluctuate more: M–N distances are identical in both $[M(\mathbf{L}')]^{2+}$ and $[M(\mathbf{L})]^{2+}$ for nickel and manganese, decrease by 0.013 Å for zinc, and by 0.021 and 0.031 Å for cobalt and copper, respectively. Other structural variables account for the full extent of the entropic changes, but these are most likely to be a distinctive signature for the better entropy of binding of manganese, nickel, and zinc to **L**. In fact, the theoretical calculations overestimated the value of $\Delta\Delta S_{theo}$ for manganese. Although experimental data show that $\Delta\Delta S_{exp}$ has an intermediate value with respect to those of Co and Cu on the one hand and Zn and Ni on the other, calculations show that manganese has the highest preference for binding to **L**. At the moment, no clear molecular picture can be deduced from our calculations to explain such discrepancies in the behavior of the manganese system.

As a result of the quantum mechanical approaches used in this work we have shown that most of the energetic properties for the metal selectivity of **L** and **L′** observed experimentally correlate to the intrinsic properties of the structures of the complexes. In particular, enthalpy essentially penalizes the binding of the metal ion to the prebinding structures of **L** compared with **L′** because of some of the constraints on the ribose moiety. These constraints are minor for the Co and Mn species. Entropy favors or penalizes binding to **L′** as a function of the modification of the metal–ligand distances and shows that Mn, Ni, and Zn are more amenable to bind to **L**. Overall we have shown that metal–ligand complementarity effects of enthalpic and/or entropic origin are in good agreement with experimental results.

Conclusions

For coordination chemists, the prediction and understanding of the coordination properties of new ligands is one of their most challenging tasks. We decided to investigate how entropic and enthalpic variables can impact on metal binding and selectivity for systems with a substantial number of degrees of freedom. To address this question, we chose a ligand **L** based on a constrained ribopyranoside scaffold and compared its coordination properties to divalent transition-metal cations with a related acyclic ligand **L′** containing the same coordinating site. We combined experimental approaches in both solution and crystalline states with computational methods, involving molecular mechanics and DFT, to study the metal-binding properties of **L** and **L′**. In this study we investigated the enthalpic and entropic impact on metal–ligand selectivity. Interestingly, both experimental and computational approaches indicated a preference for the sugar-based ligand versus its acyclic analogue, which is mainly of entropic origin. We have shown that the insertion of a sugar favors preorganized "bound-like" structures for the free ligand. The shift from $^1C_4$ to $^4C_1$ conformations is the key feature driving the coordination of the ligand. Despite the small energetic experimental and computational differences, quantum mechanics calculations show that constraints due to the ribose scaffold modulate metal binding through effects on internal entropy. These calculations do not provide exact matching between theoretical and experimental values but correlate very well with the different enthalpic and entropic trends. It is most likely that the approach used herein could have a major influence on the improvement or design of molecular scaffolds for multidentate ligands. Overall, this study shows that foreseeing both the degree of preorganization and metal–ligand complementarity for flexible systems could drive the design of new generations of chelating compounds. Sugar-derived glycoligands were considered to exemplify conformationally nontrivial ligands and are promising scaffolds for future ligand design.

Experimental Section

General Methods: Reagents and solvents were purchased from Acros and used without further purification. The synthesis of **L′** has been published elsewhere.[17] NMR analyses were performed with Bruker DRX300 and DRX400 spectrometers, and chemical shifts (δ/ppm) were calibrated relative to residual solvent signals. IR spectra were recorded with a Bruker IFS66 spectrometer and ES mass spectra with a Finnigan Mat 95S spectrometer in a *BE* configuration at low resolution. Microanalyses were performed at the CNRS (Gif-sur-Yvette and Vernaison, France). UV/Vis spectra were recorded with a Cary 300 bio spectrophotometer. Isothermal titration calorimetry was performed with a MicroCal VP-ITC device at 20 °C. Thermodynamic parameters were extracted from experimental data by using the Microcal Origin software (Origin, version 7, OriginLab Corporation, One Roundhouse Plaza, Northampton, MA 01060 USA, **2002**; with macro provided by the constructor).

Synthesis of Ribose Precursors: Compounds **1**, **2**, and **3** were synthesized according to the protocol of Jeanloz et al.[30] with very slight modifications. As these authors stated, the reaction of D-ribose with benzoyl chloride·pyridine produced a mixture of the α- and β-pyrano forms of 1,2,3,4-tetra-*O*-benzoyl-D-ribopyranose, which both yielded the β-form of the bromide. No purification of 1,2,3,4-tetra-*O*-benzoyl-D-ribopyranose was performed. 1,2-Dichloroethane used as solvent in the published procedures was replaced by dichloromethane. The unpublished NMR spectral characteristics of **1**, **2**, and **3** are reported.

2,3,4-Tri-*O*-benzoyl-β-D-ribopyranosyl Bromide (1): ^{1}H NMR (300 MHz. $CDCl_3$): δ = 8.06 (m, 3 H, H_{ar}), 7.87 (d, J = 7.1 Hz, 2 H, H_{ar}), 7.59 (m, 2 H, H_{ar}), 7.51 (t, J = 7.5 Hz, 1 H, H_{ar}), 7.33 (m, 7 H, H_{ar}), 6.70 (d, $^3J_{1,2}$ = 0.9 Hz, 1 H, 1-H), 6.15 (dd, $^3J_{2,3}$ = $^3J_{3,4}$ = 4.1 Hz, 1 H, 3-H), 5.80 (m, 2 H, 2-H, 4-H), 4.53 (dd, $^2J_{5a,5b}$ = 13.9, $^3J_{4,5a}$ = 0.9 Hz, 1 H, 5a-H), 4.35 (dd, $^2J_{5a,5b}$ = 13.9, $^3J_{4,5b}$ = 1.3 Hz, 1 H, 5b-H) ppm. ^{13}C NMR (75 MHz, $CDCl_3$): δ = 166.1, 165.8, 165.0 ($C_{q,CO}$), 133.5, 133.4, 133.3 (C_{pBz}), 130.1, 130.0, 129.8, (C_{oBz}), 129.7, 129.2, 129.1 ($C_{q,Bz}$), 128.4 (6 C, C_{mBz}), 85.8 (C-1), 71.2, 66.9, 65.5 (C-2, C-3, C-4), 64.5 (C-5) ppm.

Methyl 2,3,4-Tri-*O*-benzoyl-β-D-ribopyranoside (2): ^{1}H NMR (300 MHz. $CDCl_3$): δ = 8.06 (m, 3 H, H_{ar}), 7.87 (d, J = 7.1 Hz, 2

H, H_{ar}), 7.53 (m, 3 H, H_{ar}), 7.32 (m, 6 H, H_{ar}), 5.84 (dd, $^3J_{2,3}$ = $^3J_{3,4}$ = 3.8 Hz, 1 H, 3-H), 5.64 dd, $^3J_{2,3}$ = 3.8, $^3J_{1,2}$ = 2.3 Hz, 1 H, 2-H), 5.64 (d, $^3J_{1,2}$ = 2.3 Hz, 1 H, 1-H), 5.54 (m, 1 H, 4-H), 4.27 (dd, $^2J_{5a,5b}$ = 13.0, $^3J_{4,5a}$ = 2.1 Hz, 1 H, 5a-H), 4.12 (dd, $^2J_{5a,5b}$ = 13.0, $^3J_{4,5b}$ = 2.8 Hz, 1 H, 5b-H), 3.54 (s, 3 H, Me) ppm. ^{13}C NMR (75 MHz, $CDCl_3$): δ = 166.3, 165.8, 165.0 ($C_{q,CO}$), 133.1, 133.1 (4 C, C_{pBz}), 130.0 129.9, 129.7 (C_{oBz}), 129.7, 128.8, 128.7 ($C_{q,Bz}$), 128.4 (6 C, C_{mBz}), 99.5 (C-1), 68.7, 67.7, 66.2 (C-2, C-3, C-4), 61.1 (C-5), 55.7 (Me) ppm.

Methyl β-D-Ribopyranoside (3): ^{1}H NMR (300 MHz. CD_3OD): δ = 4.63 (d, $^3J_{1,2}$ = 3.7 Hz, 1 H, 1-H), 3.83 (dd, $^3J_{2,3}$ = $^3J_{3,4}$ = 3.0 Hz, 1 H, 3-H), 3.77 (m, 2 H, 4-H, 5a-H), 3.68 (dd, $^2J_{5a,5b}$ = 12.1, $^3J_{4,5b}$ = 5.1 Hz, 1 H, 5b-H), 3.57 (m, 1 H, 2-H), 3.42 (s, 3 H, Me) ppm. ^{13}C NMR (75 MHz, CD_3OD): δ = 100.3 (C-1), 71.1, 69.6, 65.9 (C-2, C-3, C-4), 61.1 (C-5), 55.7 (Me) ppm.

Methyl 2,3,4-Tri-*O*-picolyl-β-D-ribopyranoside (L): Compound **3** (2.5 mmol) was dissolved in DMSO (1 mL). 2-Picolyl chloride hydrochloride (9 mmol, 3.6 equiv.) was suspended in toluene (5 mL). Neutralization and concomitant extraction of 2-picolyl chloride in the toluene phase was performed by pouring satd. aq. Na_2CO_3 into this suspension until the evolution of gas had ceased. The aqueous phase was decanted, and the organic phase was added to the triol solution. $(Bu_4N)^+(HSO_4)^-$ (0.1 equiv., 0.25 mmol), *tert*-amyl alcohol (0.1 mL), and a 4:1 ground mixture of K_2CO_3/NaOH (2.5 g) were added to the reaction mixture, which was vigorously stirred overnight after which TLC analysis (AcOEt/MeOH, 9:1) showed in all cases the complete disappearance of the starting triol compound. **L** was recovered by extraction (dichloromethane/water) followed by solvent evaporation and column chromatography (elution gradient: AcOEt to AcOEt/MeOH, 9:1). Yield: 787 mg, 72%. ^{1}H NMR (400 MHz, CD_3CN): δ = 8.48 (m, $^3J_{5py,6py}$ = 4.8 Hz, 2 H, 6-H_{py}), 8.45 (d, 1 H, 6-H_{py}), 7.70–7.60 (m, 4 H), 7.49 (d, $^3J_{3py,4py}$ = 7.8 Hz, 1 H, 3-H_{py}, 5-H_{py}), 7.43 (d, $^3J_{3py,4py}$ = 7.8 Hz, 1 H, 3-H_{py}, 5-H_{py}), 7.19 (m, 3 H, 5-H_{py}), 4.85 (s_{large}, 2 H), 4.75 (m, 2 H), 4.69 (m, 2 H) (O-CH_2-py, 1-H) (sugar-ring protons: see Tables 2 and 3), 3.41 (s, 3 H, Me) ppm. ^{13}C NMR (100 MHz, CD_3CN): δ = 160.1, 159.8, 159.5 (C-2_{py}), 149.8, 149.7, 149.6 (C-6_{py}), 137.5, 137.4, 137.4 (C-4_{py}), 122.4, 122.2, 122.1, 121.4 (3 C) (C-5_{py}, C-3_{py}), 102.2 (C-1), 79.3 (C-2), 76.8 (C-3), 76.3 (C-4), 73.8, 72.9, 71.5 (*O*-CH_2-py), 64.4 (C-5), 56.5 (Me) ppm. MS (EI): *m*/*z* (%) = 460.2 (100) [**L** + Na]$^+$. IR (KBr dispersion): $\tilde{\nu}$ = 1594 ($\nu_{C=N}$), 1136, 1108, 1072 ($\delta_{py\text{-}ring}$), 762 ($\delta_{Cpy\text{-}H}$) cm^{-1}. $C_{24}H_{27}N_3O_6{\cdot}0.5H_2O$ (462.50): calcd. C 64.56, H 6.33, N 9.41; found C 64.73, H 6.24, N 9.26.

Complex Synthesis

Protocol A (M = Mn^{2+}, Zn^{2+}; Y = ClO_4^-): L (87.5, 0.2 mmol) was dissolved in absolute ethanol (2 mL). An equimolar quantity of $[M(ClO_4)_2]{\cdot}6H_2O$ was dissolved separately in absolute ethanol (1 mL). The solutions were mixed, which resulted in immediate precipitation. The precipitate was redissolved by addition of a minimal volume of acetone. Suitable crystals for X-ray diffraction analysis were obtained by slow concentration.

$[Mn(L)](ClO_4)_2{\cdot}H_2O$: MS (ES, ACN): *m*/*z* (%) = 246.1 (10) [**L** + Mn]$^{2+}$, 438.2 (3) [**L** + H]$^+$, 460.2 (100) [**L** + Na]$^+$, 591.0 (6) [**L** + Mn + ClO_4]$^+$. IR (KBr dispersion): $\tilde{\nu}$ = 1611 ($\nu_{C=N}$), 1159–1015 ($\delta_{py\text{-}ring}$, ClO_4^-), 770 ($\delta_{Cpy\text{-}H}$) cm^{-1}. $C_{24}H_{27}Cl_2MnN_3O_{13}{\cdot}1.5H_2O$ (718.36): calcd. C 40.13, H 4.04, N 5.85, Cl 9.87, Mn 7.65; found C 40.16, H 3.94, N 5.44, Cl 9.98, Mn 7.83.

$[Zn(L)](ClO_4)_2$: MS (ES, ACN): *m*/*z* (%) = 250.6 (42) [**L** + Zn]$^{2+}$, 460.2 (100) [**L** + Na]$^+$, 600.1 (15) [**L** + Mn + ClO_4]$^+$. IR (KBr dispersion): $\tilde{\nu}$ = 1612 ($\nu_{C=N}$), 1170–1020 ($\delta_{py\text{-}ring}$, ClO_4^-), 769 ($\delta_{Cpy\text{-}H}$) cm^{-1}. $C_{24}H_{27}Cl_2N_3O_{13}Zn$ (701.78): calcd. C 41.08, H 3.88, N 5.99, Cl 10.10, Zn 9.22; found C 41.22, H 3.67, N 5.81, Cl 9.48, Zn 9.08.

Protocol B (M = Co^{2+}, Ni^{2+}; Y = PF_6^-): L (87.5, 0.2 mmol) was dissolved in absolute ethanol (2 mL). An equimolar quantity of $M(NO_3)_2{\cdot}6H_2O$ was dissolved separately in absolute ethanol (1 mL). Both solutions were mixed. NH_4PF_6 (0.5 mmol, 81.5 mg, 2.5 equiv.) was dissolved in absolute ethanol (1 mL). The addition of the latter solution resulted in immediate precipitation. The precipitate was redissolved by addition of a minimal volume of acetone. Suitable crystals for X-ray diffraction analysis were obtained by slow concentration.

$[Co(L)](PF_6)_2$: MS (ES, ACN): *m*/*z* (%) = 248.1 (100) [**L** + Co]$^{2+}$, 460.2 (72) [**L** + Na]$^+$. IR (KBr dispersion): $\tilde{\nu}$ = 1609 ($\nu_{C=N}$), 1144, 1088, 1057, 1020 ($\delta_{py\text{-}ring}$), 838 (s, PF_6^-), 769 ($\delta_{Cpy\text{-}H}$) cm^{-1}. $C_{24}H_{27}CoF_{12}N_3O_5P_2$ (786.35): calcd. C 36.66, H 3.46, Co 7.49, N 5.34, P 7.88; found C 36.17, H 3.54, Co 7.31, N 5.36, P 8.11.

$[Ni(L)](PF_6)_2$: MS (ES, ACN): *m*/*z* (%) = 247.6 (42) [**L** + Ni]$^{2+}$, 438.2 (3) [**L** + H]$^+$, 460.2 (100) [**L** + Na]$^+$, 514.1 (12) [**L** + Ni + F]$^+$. IR (KBr dispersion): $\tilde{\nu}$ = 1615 ($\nu_{C=N}$), 1129, 1075, 1062, 1031 ($\delta_{py\text{-}ring}$), 838 (s, PF_6^-), 769 ($\delta_{Cpy\text{-}H}$), 556 (s, PF_6^-) cm^{-1}. $C_{24}H_{27}F_{12}N_3NiO_5P_2$ (786.11): calcd. C 36.67, H 3.46, N 5.35, Ni 7.47, P 7.88; found C 36.15, H 3.46, N 5.08, Ni 7.40, P 7.89.

X-ray Crystallography: X-ray diffraction data were collected by using a Kappa X8 APPEX II Bruker diffractometer with graphite-monochromated Mo-K_α radiation (λ = 0.71073 Å). Crystals were mounted on a CryoLoop (Hampton Research) with Paratone-N (Hampton Research) as cryoprotectant and then flash-frozen in a stream of nitrogen gas at 100 K. The temperature of the crystal was maintained at 100 K by means of a 700 series Cryostream cooling device to within an accuracy of ±1 K. The data were corrected for Lorentzian, polarization, and absorption effects. The structures were solved by direct methods using SHELXS-97[57] and refined against F^2 by full-matrix least-squares techniques using SHELXL-97[58] with anisotropic displacement parameters for all non-hydrogen atoms. Hydrogen atoms were located on a difference Fourier map and introduced into the calculations as a riding model with isotropic thermal parameters. All calculations were performed with the crystal-structure crystallographic software package WINGX.[59] The absolute configuration was determined by refining the Flack parameter[60] using a large number of Friedel pairs. The X-ray data is presented in Table S1 in the Supporting Information. CCDC-614622 {for $[Co(L)](PF_6)_2$}, -837570 {for $[Mn(L)](ClO_4)_2$}, -837571 {for $[Zn(L)](ClO_4)_2$}, -837572 (for **L**), and -837573 {for $[Ni(L)](PF_6)_2$} contain the supplementary crystallographic data for this paper. These data can be obtained free of charge from the Cambridge Crystallographic Data Centre via www.ccdc.cam.ac.uk/data_request/cif. In the case of $[Ni(L)](PF_6)_2$, the presence of four nonequivalent cationic complexes as well as disordered counteranions in the lattice did not allow the structure refinement with $R1 < 0.096$.

ITC Titrations: ITC titrations were performed at 20 °C with a MicroCal VP-ITC apparatus. Aliquots (3 μL) of the ligand solution were added to the solution of the metal salt in ethanol, which were prepared by dissolution of the $M(NO_3)_2{\cdot}6H_2O$ salts [with the exception of $Cu(NO_3)_2{\cdot}3H_2O$]. An equilibration time of 180 s was allowed between each addition. As all the complexes described in this study proved to be labile, the shape of each peak in the ITC experiment was given only by heat transfers to allow the system to reach equilibrium. The concentrations of the metal salts and of the ligands were adjusted to yield total conversion and a good signal/noise ratio for each experiment and varied between 2×10^{-5} mol L^{-1} and 10^{-3} mol L^{-1} for the metal salt and 5×10^{-4} and

2×10^{-2} mol L^{-1} for the ligand. As the ionic content of the solutions was only affected by dilution, the ratio of the activity coefficients of the solutes was assumed to be constant throughout each measurement.[61] Examples of a pair of experimental thermograms realized under the same conditions are shown in Figure S5.

Molecular Modeling. Materials and Methods: Monte Carlo calculations were performed on the ligands with the Macromodel[53] package as implemented in the Schrodinger environment.[62] By using the MCMM package, all rotational degrees of freedom, including those leading to changes in the sugar conformation, were selected as variables in the heuristic run. The force field used for these calculations is the OPLS-AA[54] (2005). For each species, 10000 cycles were performed, and a geometry optimization of 1000 steps with a gradient tolerance of 0.05 Å^2 was performed on each structure. Redundant structures were removed for rmsd values of 0.1 Å. The final sets of structures for **L′** and **L** number 8206 and 7608, respectively. To calculate the entropic quantities in the MCMM run, having defined one macrostate a as a given ensemble of relevant structures, the Boltzmann population N_j of each individual structure was calculated. The total absolute entropy of the ensemble was calculated by Equation (4).

$$S_j^a = -R\Sigma_j^a N_j \ln(N_j) \quad (4)$$

Quantum mechanical calculations were performed by using the functional density theory (DFT) with the hybrid functional B3LYP as implemented in the Gaussian 03 package.[63] Several other functionals were tested, but B3LYP gave the best agreement between optimized and experimental structures.[54,55] Moreover, B3LYP has also been reported to be a good functional for energetic reproduction of metal-binding affinities[64] and conformational study of sugar derivatives.[65] The split-valence 6-31g** basis set was used for C, N, H, and O,[66] and for metal ions the double-zeta basis set associated with the pseudopotential LANL2DZ was used.[67]

Supporting Information (see footnote on the first page of this article): Supplementary crystallographic tables and figures, supplementary figures for NMR, UV/Vis and ITC experiments, supplementary figures, tables and discussion on molecular modelling.

Acknowledgments

Financial support was provided by the French Government [ACI "Jeune Chercheur" 2004-JC4044 (to C. P.)]. J.-D. M. thanks the Spanish Ministerio de Ciencia e Innovación for funding (project no. CTQ2008-06866-C02-01 and Consolider-Ingenio 2010 no. CSD2007-00006). J.-D. M. also thanks Prof. A. Gonzalez-Lafont for her kind discussions on the Monte Carlo analysis. F. C. is grateful to the Ecole Normale Supérieure for his PhD fellowship.

[1] P. Comba, *Coord. Chem. Rev.* **1999**, *182*, 343–371; P. Comba, W. Schiek, *Coord. Chem. Rev.* **2003**, *238–239*, 21–29.
[2] R. D. Hancock, D. L. Melton, J. M. Harrington, F. C. McDonald, R. T. Gephart, L. L. Boone, S. B. Jones, N. E. Dean, J. R. Whitehead, G. M. Cockrell, *Coord. Chem. Rev.* **2007**, *251*, 1678–1689.
[3] B. P. Hay, R. D. Hancock, *Coord. Chem. Rev.* **2001**, *212*, 61–78.
[4] D. J. Cram, J. M. Cram, *Container Molecules and their Guests*, The Royal Society of Chemistry, Cambridge, **1994**; J. B. Wittenberg, L. Isaacs, in *Supramolecular Chemistry: From Molecules to Nanomaterials* (Eds.: J. W. Steed, P. A. Gale), Wiley, New Jersey, **2012**, vol. 1, pp. 25–44.
[5] P. Comba, T. W. Hambley, B. Martin, *Molecular Modeling of Inorganic Compounds*, 3rd ed., Wiley-VCH, Weinheim, **2010**.
[6] P. Comba, *Coord. Chem. Rev.* **1999**, *185–186*, 81–98; P. Comba, M. Kerscher, *Coord. Chem. Rev.* **2009**, *253*, 564–574.
[7] R. Deeth, C. Diedrich, *J. Biol. Inorg. Chem.* **2010**, *15*, 117–129; N. Gresh, G. A. Cisneros, T. A. Darden, J. P. Piquemal, *J. Chem. Theory Comput.* **2007**, *3*, 1960–1986.
[8] R. J. Deeth, A. Anastasi, C. Diedrich, K. Randell, *Coord. Chem. Rev.* **2009**, *253*, 795–816.
[9] F. W. Lichtenthaler, *Acc. Chem. Res.* **2002**, *35*, 728–737; M. J. Climent, A. Corma, S. Iborra, *Green Chem.* **2011**, *13*, 520–540.
[10] M. M. K. Boysen, *Chem. Eur. J.* **2007**, *13*, 8648–8659.
[11] S. Dhungana, J. M. Harrington, P. Gebhardt, U. Möllmann, A. L. Crumbliss, *Inorg. Chem.* **2007**, *46*, 8362–8371.
[12] The use of unprotected sugar polyols or polyolate as ligands, although not discussed here in detail, is conceptually related to our work; for a review, see: T. Allscher, P. Klüfers, P. Mayer in *Glycoscience* (Eds.: B. Fraser-Reid, K. Tatsuta, J. Thiem), Springer, Berlin, **2008**, pp. 1079–1139.
[13] I. Berger, M. Hanif, A. A. Nazarov, C. G. Hartinger, R. O. John, M. L. Kuznetsov, M. Groessl, F. Schmitt, O. Zava, F. Biba, V. B. Arion, M. Galanski, M. A. Jakupec, L. Juillerat-Jeanneret, P. J. Dyson, B. K. Keppler, *Chem. Eur. J.* **2008**, *14*, 9046–9057; M. Gottschaldt, U. S. Schubert, S. Rau, S. Yano, J. G. Vos, T. Kroll, J. Clement, I. Hilger, *ChemBioChem* **2010**, *11*, 649–652; M. Hanif, S. M. Meier, W. Kandioller, A. Bytzek, M. Hejl, C. G. Hartinger, A. A. Nazarov, V. B. Arion, M. A. Jakupec, P. J. Dyson, B. K. Keppler, *J. Inorg. Biochem.* **2011**, *105*, 224–231; M. Hanif, A. A. Nazarov, C. G. Hartinger, W. Kandioller, M. A. Jakupec, V. B. Arion, P. J. Dyson, B. K. Keppler, *Dalton Trans.* **2010**, *39*, 7345–7352; J. K. H. Hui, Z. Yu, T. Mirfakhrai, M. J. MacLachlan, *Chem. Eur. J.* **2009**, *15*, 13456–13465; R. Kikkeri, D. Grünstein, P. H. Seeberger, *J. Am. Chem. Soc.* **2010**, *132*, 10230–10232; M.-W. Louie, H.-W. Liu, M. H.-C. Lam, Y.-W. Lam, K. K.-W. Lo, *Chem. Eur. J.* **2011**, *17*, 8304–8308; Y. Mikata, S. Fujii, M. Naemura, K. Takahashi, Y. Noguchi, *Dalton Trans.* **2009**, 10305–10310; T. Shibata, H. Hashimoto, I. Kinoshita, S. Yano, T. Nishioka, *Dalton Trans.* **2011**, *40*, 4826–4829; T. Storr, L. E. Scott, M. L. Bowen, D. E. Green, K. H. Thompson, H. J. Schugar, C. Orvig, *Dalton Trans.* **2009**, 3034–3043; C.-C. Yang, P.-S. Lin, F.-C. Liu, I. J. B. Lin, G.-H. Lee, S.-M. Peng, *Organometallics* **2010**, *29*, 5959–5971; E. C. Constable, C. E. Housecroft, M. Neuburger, P. Rosel, *Chem. Commun.* **2010**, *46*, 1628–1630.
[14] M. Gottschaldt, U. S. Schubert, *Chem. Eur. J.* **2009**, *15*, 1548–1557; M. L. Bowen, C. Orvig, *Chem. Commun.* **2008**, 5077–5091.
[15] S. Woodward, M. Diéguez, O. Pàmies, *Coord. Chem. Rev.* **2010**, *254*, 2007–2030.
[16] F. Bellot, R. Hardré, G. Pelosi, M. Thérisod, C. Policar, *Chem. Commun.* **2005**, 5414–5416.
[17] G. Charron, F. Bellot, F. Cisnetti, G. Pelosi, J.-N. Rebilly, E. Rivière, A.-L. Barra, T. Mallah, C. Policar, *Chem. Eur. J.* **2007**, *13*, 2774–2782.
[18] F. Cisnetti, R. Guillot, G. Pelosi, M. Desmadril, C. Policar, *Dalton Trans.* **2007**, 1473–1476.
[19] F. Cisnetti, R. Guillot, M. Thérisod, C. Policar, *Acta Crystallogr., Sect. C* **2007**, *63*, m201–m203.
[20] F. Cisnetti, R. Guillot, N. Ibrahim, F. Lambert, M. Thérisod, C. Policar, *Carbohydr. Res.* **2008**, *343*, 530–535.
[21] F. Cisnetti, R. Guillot, M. Thérisod, M. Desmadril, C. Policar, *Inorg. Chem.* **2008**, *47*, 2243–2245.
[22] L. Garcia, S. Maisonneuve, J. Xie, R. Guillot, P. Dorlet, E. Rivière, M. Desmadril, F. Lambert, C. Policar, *Inorg. Chem.* **2010**, *49*, 7282–7288.
[23] L. Garcia, S. Maisonneuve, J. Oudinet-Sin Marcu, R. Guillot, F. Lambert, J. Xie, C. Policar, *Inorg. Chem.* **2011**, *50*, 11353–11362; C. Neff, F. Bellot, J.-B. Waern, F. Lambert, J. Brandel, G. Serratrice, F. Gaboriau, C. Policar, *J. Inorg. Biochem.* **2012**, *112*, 59–67.
[24] S. J. Angyal, *Tetrahedron* **1974**, *30*, 1695–1702; S. J. Angyal, *Chem. Soc. Rev.* **1980**, *9*, 415–428; S. J. Angyal, *Aust. J. Chem.*

2000, *53*, 567–570; B. Gyurcsick, L. Nagy, *Coord. Chem. Rev.* **2000**, *203*, 81–149; N. Nagy, A. Szorcsik, *J. Inorg. Biochem.* **2002**, *89*, 1–12; J.-F. Verchère, S. Chapelle, *Progr. Inorg. Chem.* **1998**, *47*, 837–945; D. M. Whitfield, S. Stojkovski, B. Sarkar, *Coord. Chem. Rev.* **1993**, *122*, 171–225.
[25] S. J. Angyal, *Adv. Carbohydr. Chem. Biochem.* **1989**, *47*, 1–43.
[26] N. Ghaschghaie, T. Hoffmann, M. Steinborn, P. Klufers, *Dalton Trans.* **2010**, *39*, 5535–5543; A. L. Petrou, *Coord. Chem. Rev.* **2002**, *228*, 153–162.
[27] V. J. James, J. D. Stevens, F. H. Moore, *Acta Crystallogr, Sect. B* **1978**, *34*, 188–193.
[28] R. D. Hancock, K. Hegetschweiler, *J. Chem. Soc., Dalton Trans.* **1993**, 2137–2140.
[29] In this paper, solvation issues are not discussed; however, as we consider two ligands with the same coordinating sites and their interactions with metal cations possessing the same charge, solvation effects could most confidently be neglected while discussing the metal selectivities in this study.
[30] R. Jeanloz, H. G. Fletcher, C. S. Hudson, *J. Am. Chem. Soc.* **1948**, *70*, 4052–4054.
[31] T. K. Lindhorst, *Essentials of Carbohydrate Chemistry and Biochemistry*, Wiley-VCH, Weinheim, **2003**.
[32] C. F. Macrae, P. R. Edgington, P. McCabe, E. Pidcock, G. P. Shields, R. Taylor, M. Towler, J. v. d. Streek, *J. Appl. Crystallogr.* **2006**, *39*, 453–457.
[33] R. D. Shannon, *Acta Crystallogr., Sect. A* **1976**, *32*, 751–767.
[34] D. Cremer, J. A. Pople, *J. Am. Chem. Soc.* **1975**, *97*, 1354–1358.
[35] F. E. Jorge, J. Autschbach, T. Ziegler, *J. Am. Chem. Soc.* **2005**, *127*, 975–985; E. I. Stiefel, G. F. Brown, *Inorg. Chem.* **1972**, *11*, 434–436.
[36] W. O. Gillum, R. A. D. Wentworth, R. F. Childers, *Inorg. Chem.* **1970**, *9*, 1825–1832.
[37] C. A. G. Haasnoot, F. A. A. M. de Leeuw, C. Altona, *Tetrahedron* **1980**, *36*, 2783–1792.
[38] A. D. Buckingham, *Can. J. Chem.* **1960**, *38*, 300–307.
[39] C. A. Podlasek, J. Wu, W. A. Stripe, P. B. Bondo, A. S. Serianni, *J. Am. Chem. Soc.* **1995**, *117*, 8635–8644.
[40] A. F. Cotton, G. Wilkinson, *Advanced Inorganic Chemistry*, 6th ed., Wiley-Interscience, New York, **1999**.
[41] S. Bjelić, I. Jelesarov, *J. Mol. Recognit.* **2009**, *21*, 289–312; R. J. Falconer, B. M. Collins, *J. Mol. Recognit.* **2011**, *24*, 1–16; R. J. Falconer, A. Penkova, I. Jelesarov, B. M. Collins, *J. Mol. Recognit.* **2010**, *23*, 395–413; O. Okhrimenko, I. Jelesarov, *J. Mol. Recognit.* **2008**, *21*, 1–19.
[42] D. E. Wilcox, *Inorg. Chim. Acta* **2008**, *361*, 857–867; A. Trapaidze, C. Hureau, W. Bal, M. Winterhalter, P. Faller, *J. Biol. Inorg. Chem.* **2012**, *17*, 37–47.
[43] A. Martinez, J. Suarez, T. Shand, R. S. Magliozzo, R. A. Sanchez-Delgado, *J. Inorg. Biochem.* **2011**, *105*, 39–45; S. S. Hosseini, M. Bhadbhade, R. J. Clarke, P. J. Rutledge, L. M. Rendina, *Dalton Trans.* **2011**, *40*, 506–513.
[44] E. Chekmeneva, R. Prohens, J. M. Díaz-Cruza, C. Ariñoa, M. Esteban, *Anal. Biochem.* **2008**, *375*, 82–89.
[45] G. Camci-Unal, N. L. B. Pohl, *Carbohydr. Polym.* **2010**, *81*, 8–13; S. Striegler, M. G. Gichinga, *Chem. Commun.* **2008**, 5930–5932.
[46] J.-H. Liao, C.-S. Chen, C.-C. Hu, W.-T. Chen, S.-P. Wang, I. L. Lin, Y.-H. Huang, M.-H. Tsai, T.-H. Wu, F.-Y. Huang, S.-H. Wu, *Inorg. Chem.* **2011**, *50*, 365–377; P. G. Devi, S. Pal, R. Banerjee, D. Dasgupta, *J. Inorg. Biochem.* **2007**, *101*, 127–137.
[47] M. Ostermeier, M.-A. Berlin, R. M. Meudtner, S. Demeshko, F. Meyer, C. Limberg, S. Hecht, *Chem. Eur. J.* **2010**, *16*, 10202–10213; A. H. Younes, L. Zhang, R. J. Clark, L. Zhu, *J. Org. Chem.* **2009**, *74*, 8761–8772; L. Zhang, L. Zhu, *J. Org. Chem.* **2008**, *73*, 8321–8330; N. K. Dalley, U. Olsher, J. C. Lee, M. D. Eley, J. Wang, R. A. Bartsch, *Tetrahedron* **2007**, *63*, 10576–10580; L. Mikulášek, B. Grüner, C. Dordea, V. Rudzevich, V. Böhmer, J. Haddaoui, V. Hubscher-Bruder, F. Arnaud-Neu, J. Čáslavský, P. Selucký, *Eur. J. Inorg. Chem.* **2007**, 4772–4783; P. Comba, N. Dovalil, G. Haberhauer, G. Hanson, Y. Kato, T. Taura, *J. Biol. Inorg. Chem.* **2010**, *15*, 1129–1135.
[48] H. M. Irving, R. J. P. Williams, *J. Chem. Soc.* **1953**, 3192–3210.
[49] K. Born, P. Comba, R. Ferrari, G. A. Lawrance, H. Wadepohl, *Inorg. Chem.* **2007**, *46*, 458–464.
[50] A. Bentz, P. Comba, R. J. Deeth, M. Kerscher, B. Seibold, H. Wadepohl, *Inorg. Chem.* **2008**, *47*, 9518–9527; C. Diedrich, R. J. Deeth, *Inorg. Chem.* **2008**, *47*, 2494–2506; L. Bonniard, A. de la Lande, S. Ulmer, J.-P. Piquemal, O. Parisel, H. Gérard, *Catal. Today* **2011**, *177*, 79–86; Y. D. M. Champouret, J.-D. Maréchal, I. Dadhiwala, J. Fawcett, D. Palmer, K. Singh, G. A. Solan, *Dalton Trans.* **2006**, 2350–2361.
[51] D. W. Johnson, K. N. Raymond, *Supramol. Chem.* **2001**, *13*, 639–659.
[52] J. Ali-Torres, J.-D. Maréchal, L. Rodriguez-Santiago, M. Sodupe, *J. Am. Chem. Soc.* **2011**, *133*, 15008–15014; V. Muñoz Robles, E. Ortega-Carrasco, E. G. Fuentes, A. Lledos, J.-D. Maréchal, *Faraday Discuss.* **2011**, *148*, 137–159.
[53] F. Mohamadi, N. G. J. Richard, W. C. Guida, L. R. M. Lipton, C. Caufield, G. Chang, T. Hendrickson, W. C. Still, *J. Comput. Chem.* **1990**, *11*, 440–467.
[54] W. Jorgensen, D. Maxwell, J. Tirado-Rives, *J. Am. Chem. Soc.* **1996**, *118*, 11225–11236.
[55] A. D. Becke, *J. Chem. Phys.* **1993**, *98*, 5648–5652.
[56] C. Lee, W. Yang, R. G. Parr, *Phys. Rev. B* **1988**, *37*, 785–789.
[57] G. Sheldrick, *SHELXS-97, Program for Crystal Structure Refinement*, University of Göttingen, Göttingen, **1997**.
[58] G. Sheldrick, *SHELXL-97 Program for Crystal Structure Refinement*, University of Göttingen, Göttingen, **1997**.
[59] L. J. Farrugia, *J. Appl. Crystallogr.* **1999**, *32*, 837–838.
[60] H. D. Flack, *Acta Crystallogr., Sect. A* **1983**, *39*, 876–881.
[61] M. Miguirditchian, D. Guillaneux, D. Guillaumont, P. Moisy, C. Madic, M. P. Jensen, K. L. Nash, *Inorg. Chem.* **2005**, *44*, 1404–1412.
[62] *Macromodel*, version 9.5, Schrödinger, LCC, New York, **2011**, and *Maestro*, version 9.2, Schrödinger, LLC, New York, NY, **2011**.
[63] M. J. Frisch, G. W. Trucks, H. B. Schlegel, G. E. Scuseria, M. A. Robb, J. R. Cheeseman, J. A. Montgomery Jr., T. Vreven, K. N. Kudin, J. C. Burant, J. M. Millam, S. S. Iyengar, J. Tomasi, V. Barone, B. Mennucci, M. Cossi, G. Scalmani, N. Rega, G. A. Petersson, H. Nakatsuji, M. Hada, M. Ehara, K. Toyota, R. Fukuda, J. Hasegawa, M. Ishida, T. Nakajima, Y. Honda, O. Kitao, H. Nakai, M. Klene, X. Li, J. E. Knox, H. P. Hratchian, J. B. Cross, V. Bakken, C. Adamo, J. Jaramillo, R. Gomperts, R. E. Stratmann, O. Yazyev, A. J. Austin, R. Cammi, C. Pomelli, J. W. Ochterski, P. Y. Ayala, K. Morokuma, G. A. Voth, P. Salvador, J. J. Dannenberg, V. G. Zakrzewski, S. Dapprich, A. D. Daniels, M. C. Strain, O. Farkas, D. K. Malick, A. D. Rabuck, K. Raghavachari, J. B. Foresman, J. V. Ortiz, Q. Cui, A. G. Baboul, S. Clifford, J. Cioslowski, B. B. Stefanov, G. Liu, A. Liashenko, P. Piskorz, I. Komaromi, R. L. Martin, D. J. Fox, T. Keith, M. A. Al-Laham, C. Y. Peng, A. Nanayakkara, M. Challacombe, P. M. W. Gill, B. Johnson, W. Chen, M. W. Wong, C. Gonzalez, J. A. Pople, *Gaussian 03*, revision D.01, Gaussian, Wallingford, CT, **2004**.
[64] T. Marino, N. Russo, M. Toscano, *J. Inorg. Biochem.* **2000**, *79*, 179–185; J. Bertran, L. Rodriguez-Santiago, M. Sodupe, *J. Phys. Chem. B* **1999**, *103*, 2310–2317.
[65] G. L. Strati, J. L. Willett, F. A. Momany, *Carbohydr. Res.* **2002**, *337*, 1833–1849.
[66] W. J. Hehre, R. Ditchfield, J. A. Pople, *J. Chem. Phys.* **1972**, *56*, 2257–2261; P. C. Hariharan, J. A. Pople, *Theor. Chim. Acta* **1973**, *28*, 213–222.
[67] P. J. Hay, W. R. Wadt, *J. Chem. Phys.* **1985**, *82*, 299–310.

Received: March 27, 2012
Published Online: May 29, 2012

